INTERNATIONAL JOURNAL OF WATER TECHNOLOGY AND TREATMENT METHODS

A Novel Boron Nitride-Graphene Oxide Thin Film Nanocomposites Modified with Multiwalled Carbon Nanotubes Functionalized with Carboxyl Groups Membrane in the Efficient Removal of Ciprofloxacin in Pharmaceutical Industry Wastewater

Öztekin R and Sponza DT*

Dokuz Eylül University, Engineering Faculty, Department of Environmental Engineering, Tınaztepe Campus, 35160 Buca/Izmir, Turkey

Article Information

Article Type: Research Article
Journal Type: Open Access
Volume: 1 Issue: 1
Manuscript ID: IJWTTM-v1-103
Publisher: Science World Publishing

***Corresponding Author:**

Delia Teresa Sponza,
Dokuz Eylül University, Engineering Faculty, Department of Environmental Engineering, Tınaztepe Campus, 35160 Buca/Izmir, Turkey,
Tel. +90 232 301 7119;
Fax: + 90 232 453 11 43;
E-mail: delya.sponza@deu.edu.tr

Citation:
Sponza DT (2023).
A Novel Boron Nitride-Graphene Oxide Thin Film Nanocomposites Modified with Multiwalled Carbon Nanotubes Functionalized with Carboxyl Groups Membrane in the Efficient Removal of Ciprofloxacin in Pharmaceutical Industry Wastewater.
I J Water Tech Treat Methods, 1(1);1-20

Recieved Date: 16 Jan 2023
Accepted Date: 15 Mar 2023
Published Date: 25 Mar 2023

Abstract

In this study, a novel boron nitride-graphene oxide thin film nanocomposites (BN/GO NCs) modified with multiwalled carbon nanotubes functionalized with carboxyl groups (MWCNT-COOH) membrane was examined during electrochemical filtration process in the efficient removal of ciprofloxacin (CIP) in pharmaceutical industry wastewater, İzmir, Turkey. Different pH values (2.5, 3.5, 5.5, 7.0, 9.0 and 11.0), increasing CIP concentrations (5 mg/l, 15 mg/l, 45 mg/l and 60 mg/l), different GO/BN NCs mass ratios (8/1, 4/1, 2/1, 1/1, 1/2, 1/4 and 1/8), increasing recycle time (1., 2., 3., 4., 5., 6. and 7.) was operated during electrochemical filtration process in the efficient removal of CIP in pharmaceutical industry wastewater. The characteristics of the synthesized nanoparticles were assessed using X-Ray Difraction (XRD), Field Emission Scanning Electron Microscopy (FESEM), Energy-Dispersive X-Ray (EDX), Fourier Transform Infrared Spectroscopy (FTIR), Transmission Electron Microscopy (TEM), and Diffuse reflectance UV-Vis spectra (DRS) analyses, respectively. The acute toxicity assays were operated with Microtox (Aliivibrio fischeri also called Vibrio fischeri) and Daphnia magna acute toxicity tests. ANOVA statistical analysis was used for all experimental samples. The maximum 97% CIP removal efficiency was obtained with the multiwalled carbon nanotubes functionalized with carboxyl groups/boron nitrite-nanosheets/graphene oxide (MWCNT/BN-NSs/GO) membrane during electrochemical filtration process in pharmaceutical industry wastewater, at pH=9.0 and at 25oC, respectively. The maximum 99% CIP removal efficieny was found with the MWCNT/BN-NSs/GO membrane during electrochemical filtration process in pharmaceutical industry wastewater, at 5 mg/l CIP, at pH=9.0 and at 25oC, respectively. The maximum 99% CIP removal efficiency was obtained with the MWCNT/BN-NSs/GO membrane during electrochemical filtration process in pharmaceutical industry wastewater, at 1/2 GO/BN NCs mass ratio, at 5 mg/l CIP, at pH=9.0 and at 25oC, respectively. The maximum 99% CIP removal efficiency was obtained with the MWCNT/BN-NSs/GO membrane during electrochemical filtration process in pharmaceutical industry wastewater, after 1. recycle time, at 5 mg/l CIP, at pH=9.0 and at 25oC, respectively. 94.44% maximum Microtox acute toxicity yield was found in CIP=45 mg/l after 150 min electrochemical filtration time and at 60oC, respectively. 90%

maximum Daphnia magna acute toxicity removal was obtained in CIP=45 mg/l after 150 min electrochemical filtration time and at 60oC, respectively. As a result, it can be concluded that the toxicity originating from the CIP is not significant and the real acute toxicity throughout electrochemical filtration process was attributed to the pharmaceutical industry wastewater, to their metabolites and to the electrochemical filtration by-products. Finally, the MWCNT/BN-NSs/GO membrane during electrochemical filtration process in pharmaceutical industry wastewater was stable in harsh environments such as acidic, alkaline, saline, and then was still effective process. When the amount of contaminant was increased, the MWCNT/BN-NSs/GO membrane performance was still considerable. Finally, the combination of a simple, easy operation preparation process and excellent performance makes this MWCNT/BN-NSs/GO membrane a promising option during electrochemical filtration process in pharmaceutical industry wastewater treatment.

Keywords: ANOVA statistical analysis; Antibiotic; Ciprofloxacin; DRS: Diffuse reflectance UV-Vis spectra; Electrochemical filtration process; EDX: Energy-dispersive X-ray; FESEM: Field emission scanning electron microscopy; FTIR: Fourier transform infrared spectroscopy; Graphene oxide-Boron nitride thin film novel nanocomposite; Microtox (Aliivibrio fischeri or Vibrio fischeri) and Daphnia magna acute toxicity tests; Multiwalled Carbon Nanotubes Functionalized with Carboxyl Groups; Pharmaceutical industry wastewater; TEM: Transmission Electron Microscopy; XRD: X-ray difraction

Introduction

Emerging contaminants (ECs), sometimes known as contaminants of emerging concern (CECs) can refer to a wide variety of artificial or naturally occurring chemicals or materials that are harmful to human health after long-term disclosure. ECs can be classified into several classes, including agricultural contaminants (pesticides and fertilizers), medicines and antidote drugs, industrial and consumer waste products, and personal care and household cleaning products (Idham et al., 2017; Idham et al., 2021). Antibiotics are one of the ECs that have raised concerns in the previous two decades because they have been routinely and widely used in human and animal health care, resulting in widespread antibiotic residues discharged in surface, groundwater, and wastewater.

Antibiotics, which are widely utilized in medicine, poultry farming and food processing (Arenas and Melo, 2018; Pellerito et al., 2018), have attracted considerable attention due to their abuse and their harmful effects on human health and the ecological environment (Fridkin et al., 2014; Tamma et al., 2017). The misuse of antibiotics induces Deoxyribonucleic Acid (DNA) contamination and accelerates the generation of drug-resistant bacteria and super-bacteria (Huo, 2010; Ferri et al., 2017; Tan et al., 2018); thus, some diseases are more difficult to cure (Tong et al., 2018). A number of studies have revealed that the level of antibiotics in the soil, air and surface water, and even in potable water, is excessive in many areas (Alygizakis et al., 2016; Casanova and Sobsey, 2016; Zhang et al., 2016), which will ultimately accumulate in the human body via drinking water and then damage the body's nervous system, kidneys and blood system. Therefore, it is necessary to develop an efficient method to remove antibiotics present in pharmaceutical industry wastewater.

The uncontrolled, ever-growing accumulation of antibiotics and their residues in the environment is an acute modern problem. Their presence in water and soil is a potential hazard to the environment, humans, and other living beings. Many therapeutic agents are not completely metabolized, which leads to the penetration of active drug molecules into the biological environment, the emergence of new contamination sources, the wide spread of bacteria and microorganisms with multidrug resistance (Jiménez-Tototzintle et al., 2018; Kerrigan, et al., 2018; McConnell et al., 2018). Modern pharmaceutical wastewater facilities do not allow efficient removal of antibiotic residues from the environment (Karthikeyan and Meyer, 2006; Dinh et al., 2017), which leads to their accumulation in ecological systems (Dong et al., 2016; Siedlewicz et al., 2018). Global studies of river pollution with antibiotics have shown that 65% of surveyed rivers in 72 countries on 6 continents are contaminated with antibiotics (Barry, 2019). According to the World Health Organization (WHO), surface and groundwater, as well as partially treated water, containing antibiotics residue and other pharmaceuticals, typically at < 100 ng/l concentrations, whereas treated water has < 50 ng/l concentrations, respectively (Maycock and Watts, 2011). However, the discovery of ECs in numerous natural freshwater sources worldwide is growing yearly. Several antibiotic residues have been reported to have been traced at concentrations greater than their ecotoxicity endpoints in the marine environment, specifically in Europe and Africa (Fekadu et al., 2019). Thus, the European Union's Water Framework Directive enumerated certain antibiotics as priority contaminants (Wang et al., 2017a; Wang et al., 2017b). In some rivers, the concentrations were so high that they posed a real danger to both the ecosystem and human health. This matter, the development of effective approaches to the removal of antibiotics from the aquatic environment is of great importance.

The removal of antibiotics and their residues from water and wastewater prior to their final release into the environment is of particular concern (Yang et al., 2021). Modern purification methods can be roughly divided into the following three categories depending on the purification mechanism: biological treatment (Akyon et al., 2019; Zhang et al., 2019), chemical degradation (de Souza Santos et al., 2015; Yang et al., 2021), and physical removal. Each of these methods has its own advantages and disadvantages.

For example, biological purification can remove most antibiotic residues, but the introduction of active organisms into the aquatic environment can upset the ecological balance. Various chemical approaches (ozonation, chlorination, and Fenton oxidation) cannot provide complete purification and, in some cases, lead to the death of beneficial microorganisms due to low selectivity. Photocatalysis is widely used in new environmental control strategies (Zhong et al., 2018; Alagha et al., 2021; Yang et al., 2022). However, this method has a number of key disadvantages, such as insufficient use of visible light, rapid annihilation of photogenerated carriers, and incomplete mineralization, which greatly limits its application (Yang et al., 2021).

Ciprofloxacin (CIP) is an antibiotic belonging to the second-generation fluoroquinolones, which can treat different bacterial infections (Fang et al., 2021; Kaur Sodhi and Kumar Singh, 2021). The entrance of this substance into the nature can cause bacterial drug resistance. Recently, studies have reported the presence of CIP residuals in aqueous resources and effluent of wastewater treatment plants (Tamaddon et al., 2020; Firouzeh et al., 2021). Unfortunately, the conventional methods cannot remove CIP completely, therefore, newer methods should be investigated (Gupta et al., 2021). Advanced oxidation processes (AOPs) have recently been introduced as a promising option for the removal of CIP from aqueous media (Malakootian et al., 2019).

Numerous materials have been reported to have the potential and capacity to treat water or wastewater polluted with these antibiotics residue by applying the processes of adsorption and catalytic oxidation during the last few decades. The reported materials include mesoporous carbon beads (Ahammad et al., 2021), biochar (Li et al., 2017; Jiang et al., 2020; Shirani et al., 2020), clay minerals (Ahmed et al., 2015), activated carbon (Zhang et al., 2020; Avcu et al., 2021; Ji et al., 2022), cellulose (Shahnaz et al., 2021; Wang et al., 2021), and chitosan (Cui et al., 2019; Phasuphan et al., 2019; ALOthman et al., 2020). As a result of engineering and science evolution, and in complement to the urgent need to increase the adsorption capability of antibiotic contaminants, more advanced materials such as carbon nanotube (CnT) (Yu et al., 2016; Zhao et al., 2016; Bellamkonda et al., 2019; Rigueto et al., 2021), nano-zero valent iron (nZVI) (Ahmed et al., 2017; Zhao et al., 2020; Nguyen et al., 2020; Nyugen et al., 2021; Falyouna et al., 2022a; Falyouna et al., 2022b), nanoporous carbons (Mokhati et al., 2021), porous graphene (Shan et al., 2017; Khalil et al., 2020) and graphene oxide (GO) (Görmez et al., 2019; Qiao et al., 2020; Idham et al., 2021; Nguyen et al., 2021), to date have been analyzed and improved in their ability to remove these ECs from water.

Nanomaterials with a high specific surface area are a promising platform for the development and production of low-cost and highly efficient sorbents for various pollution molecules (Yadav et al., 2021; Liu et al., 2022). For example, graphene-based nanomaterials were utilized to remove antibiotics (Bao, et al., 2018; Tang et al., 2019; Wang et al., 2019), which are adsorbed on the material surfaces due to π-π-, electrostatic or hydrophobic interactions, as well as the formation of hydrogen bonds. Highly efficient antibiotic sorption was also observed when using highly porous, surface-active, and structurally stable silica-based materials (Masoudi et al., 2019; Zeidman et al., 2020), metal oxide nanoparticles (NPs) (Alagha et al., 2021; Sturini et al., 2021; Li et al., 2022), and metal-organic frameworks (Dehghan et al., 2019; Sun et al., 2021).

Graphene oxide (GO), one of the carbon nanomaterials, has piqued the widespread attraction of environmental specialists worldwide in recent years since it was first exfoliated from graphite in 2004 (Liu et al., 2021). This material has been proven as a prospective material for treating water contaminated with ECs (Idham et al., 2017). With its superior mechanical qualities and unique physicochemical features, GO promises a significant adsorption impact when employed alone or as a supporting material, particularly in water treatment applications (Peng et al., 2017).

Boron nitride (BN), another 2D nanomaterial which is known as "white graphene", has unique properties distinct from graphene. Its characteristics include strong oxidation resistance at high temperatures, excellent adsorption capability, no surface charge and special luminescence. BN nanosheets are remarkable substrates for graphene, MoS2 layers and other 2D nanomaterials in electronic and optical applications. Recently, BN has been widely used in membrane research area (Razmjou et al., 2012; Liu et al., 2017; Abdikheibari et al., 2018; Gonzalez-Ortiz et al., 2018). Due to the unique combination of physicochemical properties, hexagonal boron nitride (h-BN) finds application in the following various fields: physics, chemistry, materials science, and biomedicine (Tang et al., 2006; Dai et al., 2015; Gudz et al., 2020). Its high specific surface area and superior thermal and chemical stability determine its attractiveness as an effective sorbent. The polarity of the BN bonds and the large surface area provide good adsorption properties for various substances, from organic pollutants (Zhang et al., 2012) to hydrogen (Portehault et al., 2010). Since BN nanostructures are very light, BN-based sorbents have a high gravimetric capacity, and their high chemical and thermal stability ensure good material regeneration. Hexagonal BN mesoporous fibers (Xue et al., 2014) and h-BN porous whiskers (Li et al., 2016) showed a high degree of sorption of organic colorants (> 631 mg/g). Cotton flower-like porous BN (Maiti et al., 2017) and stamen-shaped porous boron carbon nitride nanoscrolls (Wang et al., 2017) also demonstrated highly efficient removal of contaminants. Hollow BN NPs can serve as a reservoir of boron for the treatment of prostate cancer (Li et al., 2017).

Recently, two-dimensional (2D) nanomaterials, such as GO (Co-

hen-Tanugi and Grossman, 2012; Mi, 2014; Homaeigohar and Elbahri, 2017), BN (Falin et al., 2017; Fan et al., 2017), transition metal dichalcogenides (Pan et al., 2016; Shi et al., 2016; Hirunpinyopas et al., 2017), have been investigated in the membrane process due to their particular physical and chemical properties. For example, GO is appropriate for fabricating filter membranes due to its atomic thin thickness, lamellar structure and consequent specific properties, such as high chemical stability and specific surface, and its porous and rich oxygen-containing functional sites (Fathizadeh et al., 2017). Moreover, GO-based membranes, using tunable interlayer spacing to intercept ions and contaminants in water, are most promising (Mi, 2014; Cheng et al., 2016; Jiao et al., 2017; Tang et al., 2018). However, GO membranes do have some deficiencies. A number of methods and experiments have been performed to overcome the weaknesses of the original GO membrane, such as swelling or delamination in aqueous solutions and the tradeoff between selectivity and permeability (Park et al., 2017).

The detection and quantification of CIP is based on traditional analytical methods, such as: high-performance liquid chromatography (HPLC), liquid chromatography coupled with tandem mass spectrometry (LC-MS), ultraviolet (UV) detection and capillary electrophoresis (CE). These techniques have high sensitivity and accuracy, they are time consuming and require expensive and complicated equipment, thus limiting their application in routine analysis. These methods require the use of potentially harmful solvents, the need for training, and certified operators. These methods are limited in terms of on-site, instantaneous and in situ analyses (Kumunda et al., 2021). Chromatographic procedures usually offer lower detection limits, electrochemical methods can be an interesting alternative due to their simplicity, short operating time, low cost and small amount of waste generation (Swapna Priya and Radha, 2017; Teodosiu et al., 2018). The ease of electrochemical methods in operation, rapid analytical response, absence of pretreatment sample, technically miniaturized and portable devices, make them accessible for on-site analysis (Silwana et al., 2016; Bansod et al., 2017; Smith et al., 2019). The use of electrochemical methods as well as electrochemical sensors have allowed the using a carbon paste electrode modified with a combination of multiwalled carbon nanotubes functionalized with carboxyl groups (MWCNT-COOH) (Wong et al., 2015). Electrochemical filtration process integrates degradation and separation of contaminants. Filter pore size is well controlled using NPs as a filler. Double-sheet filter designs are more efficient than single-sheet in fouling control. Electrocatalytic filters achieve simultaneous removal of organics and particulates.

In this study, a novel BN/GO NCs modified with MWCNT-COOH membrane was examined during electrochemical filtration process in the efficient removal of CIP in pharmaceutical industry wastewater plant, İzmir, Turkey. Different pH values (2.5, 3.5, 5.5, 7.0, 9.0 and 11.0), increasing CIP concentrations (5 mg/l, 15 mg/l, 45 mg/l and 60 mg/l), different GO/BN NCs mass ratios (8/1, 4/1, 2/1, 1/1, 1/2, 1/4 and 1/8), increasing recycle time (1., 2., 3., 4., 5., 6. and 7.) was operated during electrochemical filtration process in the efficient removal of CIP in pharmaceutical industry wastewater. The characteristics of the synthesized NPs were assessed using XRD, FESEM, EDX, FTIR, TEM and DRS analyses, respectively. The acute toxicity assays were operated with Microtox (Aliivibrio fischeri or Vibrio fischeri) and Daphnia magna acute toxicity tests. ANOVA statistical analysis was used for all experimental samples.

Materials and Methods

Characterization of Pharmaceutical Industry Wastewater

Characterization of the biological aerobic activated sludge proses from a pharmaceutical industry wastewater plant, İzmir, Turkey was performed. The results are given as the mean value of triplicate samplings (Table 1).

Table 1: Characterization of Pharmaceutical Industry Wastewater

Parameters	Unit	Concentrations
Chemical oxygen demand-total (COD_{total})	(mg/l)	4000
Chemical oxygen demand-dissolved ($COD_{dissolved}$)	(mg/l)	3200
Biological oxygen demand-5 days (BOD_5)	(mg/l)	1500
BOD_5 / $COD_{dissolved}$		0.5
Total organic carbons (TOC)	(mg/l)	1800
Dissolved organic carbons (DOC)	(mg/l)	1100
pH		8.3
Salinity as Electrical conductivity (EC)	(mS/cm)	1552
Total alkalinity as $CaCO_3$	(mg/l)	750
Total volatile acids (TVA)	(mg/l)	380
Turbidity (Nephelometric Turbidity unit, NTU)	NTU	7.2
Color	1/m	50
Total suspended solids (TSS)	(mg/l)	250

Volatile suspended solids (VSS)	(mg/l)	187
Total dissolved solids (TDS)	(mg/l)	825
Nitride (NO_2^-)	(mg/l)	1.7
Nitrate (NO_3^-)	(mg/l)	1.91
Ammonium (NH_4^+)	(mg/l)	2.3
Total Nitrogen (Total-N)	(mg/l)	3.2
SO_3^{-2}	(mg/l)	21.4
SO_4^{-2}	(mg/l)	29.3
Chloride (Cl^-)	(mg/l)	37.4
Bicarbonate (HCO_3^-)	(mg/l)	161
Phosphate (PO_4^{-3})	(mg/l)	16
Total Phosphorus (Total-P)	(mg/l)	40
Total Phenols	(mg/l)	70
Oil & Grease	(mg/l)	220
Cobalt (Co^{+3})	(mg/l)	0.2
Lead (Pb^{+2})	(mg/l)	0.4
Potassium (K^+)	(mg/l)	17
Iron (Fe^{+2})	(mg/l)	0.42
Chromium (Cr^{+2})	(mg/l)	0.44
Mercury (Hg^{+2})	(mg/l)	0.35
Zinc (Zn^{+2})	(mg/l)	0.11

Preparation of GO Nanoparticles Dispersion

GO NPs was prepared using the modified Hummers' method (Hummers and Offeman, 1958). A mixed solution of concentrated 60 ml H_2SO_4, 4.2 g $K_2S_2O_8$ and 4.2 g P_2O_5 was heated to 80°C, and 5 g graphite powder was added under continuous stirring for 4.5 h. When the solution had cooled, the products obtained were filtered and washed with deionized water until no residual acid was present. 5 g dried fluffy product was then placed into concentrated 120 ml H_2SO_4 at 0°C, followed by the controlled addition of 2.5 g KNO_3 and 16 g $KMnO_4$ with the temperature < 10°C. The reaction was performed at 35°C for 2 h, and continued for a further 2 h following the addition of 250 ml deionized water. After, 600 ml deionized water and 30 ml H_2O_2 (30 wt%) were added to the solution, and allowed to stand overnight. Finally, the mixture was washed with 1 M HCl solution and deionized water to confirm the removal of metal ions and acid, then dried at 60°C for 2 days (48 h). As a result, 2 mg/ml GO suspension was obtained after sonication, and used in this study.

Preparation of Boron Nitride-Nanosheets (BN-NSs) Dispersion

BN-NSs dispersion was prepared using commercial h-BN powder by ball milling (planetary ball mill, QM-3SP2) (Lei et al., 2015). 0.5 g h-BN powder and 30 g urea (CH_4N_2O) were added to a ball mill cell and ball milled at 500 rpm for 12 h at room temperature. During the high-energy ball-milling process, BN and CH_4N_2O particles were thoroughly mixed, and some small CH_4N_2O molecules may intercalate into the BN structure from the edges of BN layers. Powered by the energy of colliding balls, CH_4N_2O would decompose and lead to chemical bonding of NH_2 group to few-layer BN. After ball milling, the product was washed with deionized water to remove CH_4N_2O. The collected BN-NSs was dispersed in water by sonication, then the dispersion was centrifuged for 30 min at 2000 rpm. The supernatant was collected and filtrated to obtain BN-NSs. Finally, 2 mg/ml BN nanosheets dispersion was prepared by dispersing solid BN-NSs in water. The dispersion was then characterized by zeta potential, FESEM and TEM analysis. BN-NSs dispersion used below was all 2 mg/ml.

Preparation of the Multiwalled Carbon Nanotubes Functionalized with Carboxyl Groups/ Boron Nitride Nanosheets/Graphene Oxide (MWCNT-COOH/BN-NSs/GO) Membrane

6 ml MWCNT-COOH dispersion was added into 2 ml GO dispersion and stirring for 10 min, then 4 ml BN-NSs dispersion was dropped into mixed solution under stirring. The final mixed solution was stirred at room temperature for 10 min, followed by sonication for 10 min, repeated 6 times. After, the mixed dispersion was used to prepare the 15 mg MWCNT-COOH/BN-NSs/GO membranes on a PVDF (polyvinylidene fluoride) membrane through vacuum filtration. The prepared membrane was used to filter the CIP solution and was characterized by SEM, TEM and XRD analysis. 3 mg MWCNT-COOH and 12 mg BN-NSs/GO NCs was constant. BN-NSs/GO NCs mass ratio was changed to 8/1, 4/1, 2/1, 1/1, 1/2, 1/4 and 1/8 to optimize the performance of the membrane. 2 ml GO

NPs dispersion was used to prepare pure GO NPs membrane. 4 ml BN-NSs NPs dispersion was used to prepare pure BN-NSs NPs membrane. MWCNT-COOH/GO membrane was produced by 2 ml GO NPs dispersion + 6 ml MWCNT-COOH dispersion. Pure GO NPs and pure BN-NSs NPs were modified with MWCNT-COOH groups. MWCNT-COOH/BN-NSs/GO membrane were produced to detect their performance for the efficient removal of CIP from pharmaceutical industry wastewater.

Electrochemical Filtration of CIP from MWCNT-COOH/BN-NSs/GO Membrane

Seven MWCNT-COOH/BN-NSs/GO membranes (each of 15 mg) were prepared under the same conditions. GO NPs to BN-NSs NPs mass ratio in MWCNT-COOH/BN-NSs/GO membrane was changed. The prepared MWCNT-COOH/BN-NSs/GO membranes were used to filter 36 mg/l CIP solution by vacuum filtration and the vacuum degree was stabilized at 0.9 atm pressure. CIP solution volume was 20 ml. The filter liquor was collected and detected by ultraviolet-visible (UV-Vis) spectroscopy. The rejection to CIP using the prepared MWCNT-COOH/BN-NSs/GO membrane was calculated by the following as Equation 1:

$$\eta = \frac{(C_0 - C)}{C_0} x\ 100\ (\%) = \frac{(A_0 - A)}{A_0} x\ 100\ (\%) \quad (1)$$

where; η: is the membrane rejection, C_0 and C: are CIP solution concentrations before and after filtration, A_0 and A: are CIP maximal absorbance before and after filtration.

The permeance of the membrane was calculated by the following as Equation 2:

$$J = \frac{V}{(S\ x\ T\ x P)} \quad (2)$$

where; J: is the membrane permeance, V: is CIP solution volume, S: is the membrane area, T: is the filtration time and P: is the vacuum degree.

Different NaCl and $CaCl_2$ solution concentrations (from 0.1 to 1.0 mol/l) were prepared to measure the effect of salts to the MWCNT-COOH/BN-NSs/GO membrane performance. The collected data were averages of three parallel tests. Three MWCNT-COOH/BN-NSs/GO membranes were prepared for each condition at the same time.

Characterization

X-Ray Diffraction Analysis: Powder XRD patterns were recorded on a Shimadzu XRD-7000, Japan diffractometer using Cu Kα radiation (λ = 1.5418 Å, 40 kV, 40 mA) at a scanning speed of 1° /min in the 10-80° 2θ range. Raman spectrum was collected with a Horiba Jobin Yvon-Labram HR UV-Visible NIR (200-1600 nm) Raman microscope spectrometer, using a laser with the wavelength of 512 nm. The spectrum was collected from 10 scans at a resolution of 2 /cm. The zeta potential was measured with a SurPASS Electrokinetic Analyzer (Austria) with a clamping cell at 300 mbar.

Field Emission Scanning Electron Microscopy (FESEM) and Energy Dispersive X-Ray (EDX) Spectroscopy Analysis: The morphological features and structure of the synthesized catalyst were investigated by FESEM (FESEM, Hitachi S-4700), equipped with an EDX spectrometry device (TESCAN Co., Model III MIRA) to investigate the composition of the elements present in the synthesized catalyst.

Fourier Transform Infrared Spectroscopy (FTIR) Analysis: The FTIR spectra of samples was recorded using the FT-NIR spectroscope (RAYLEIGH, WQF-510).

Transmission Electron Microscopy (TEM) Analysis: The structure of the samples were analysed TEM analysis. TEM analysis was recorded in a JEOL JEM 2100F, Japan under 200 kV accelerating voltage. Samples were prepared by applying one drop of the suspended material in ethanol onto a carbon-coated copper TEM grid, and allowing them to dry at 25°C room temperature.

Diffuse Reflectance UV-Vis Spectra (DRS) Analysis: DRS Analysis in the range of 200–800 nm were recorded on a Cary 5000 UV-Vis Spectrophotometer from Varian. DRS was used to monitor the CIP antibiotic concentration in experimental samples.

Analytical Procedures

Chemical oxygen demand-total (COD_{total}), chemical oxygen demand-dissolved ($COD_{dissolved}$), total phosphorus (Total-P), phosphate phosphorus (PO_4^{-3}-P), total nitrogen (Total-N), ammonium nitrogen (NH_4^+-N), nitrate nitrogen (NO_3^--N), nitrite nitrogen (NO_2^--N), biological oxygen demand 5-days (BOD_5), pH, Temperature [(°C)], total suspended solids (TSS), total volatile suspended solids (TVSS), total organic carbon (TOC), Oil, Chloride (Cl^-), total phenol, total volatile acids (TVA), disolved organic carbon (DOC), total alkalinity, turbidity, total dissolved solid (TDS), color, sulfide (SO_3^{-2}), sulfate (SO_4^{-2}), bicarbonate (HCO_3^-), salinity, cobalt (Co^{+3}), lead (Pb^{+2}), potassium (K^+), iron (Fe^{+2}), chromium (Cr^{+2}), Mercury (Hg^{+2}) and zinc (Zn^{+2}) were measured according to the Standard Methods (2017) 5220B, 5220D, 4500-P, 4500-PO_4^{-3}, 4500-N, 4500-NH_4^+, 4500-NO_3^-, 4500-NO_2^-, 5210B, 4500-H^+, 2320, 2540D, 2540E, 5310, 5520, 4500-Cl^-, 5530, 5560B, 5310B, 2320, 2130, 2540E, 2120, 4500-SO_3^{-2}, 4500-SO_4^{-2}, 5320, 2520, 3500-Co^{+3}, 3500-Pb^{+2}, 3500- K^+, 3500-Fe^{+2}, 3500-Cr^{+2}, 3500-Hg^{+2}, 3500-Zn^{+2}, respectively (Baird et al., 2017).

Total-N, NH_4^+-N, NO_3^--N, NO_2^--N, Total-P, PO_4^{-3}-P, total phenol, Co^{+3}, Pb^{+2}, K^+, Fe^{+2}, Cr^{+2}, Hg^{+2}, Zn^{+2}, SO_3^{-2}, and SO_4^{-2} were measured with cell test spectroquant kits (Merck, Germany) at a spectroquant NOVA 60 (Merck, Germany) spectrophotometer (2003).

The measurement of color was carried out following the methods described by Olthof and Eckenfelder (1976) and Eckenfelder (1989). According these methods, the color content was determined by measuring the absorbance at three wavelengths (445 nm, 540 nm and 660 nm), and taking the sum of the absorbances at

these wavelengths. In order to identify the color in pharmaceutical industry wastewater (25 ml) was acidified at pH=2.0 with a few drops of 6 N HCl and extracted three times with 25 ml of ethyl acetate. The pooled organic phases were dehydrated on sodium sulphate, filtered and dried under vacuum. The residue was sylilated wit bis(trimethylsylil)trifluoroacetamide (BSTFA) in dimethylformamide and analyzed by gas chromatography–mass spectrometry (GC-MS) and gas chromatograph (GC) (Agilent Technology model 6890N) equipped with a mass selective detector (Agilent 5973 inert MSD). Mass spectra were recorded using a VGTS 250 spectrometer equipped with a capillary SE 52 column (HP5-MS 30 m, 0.25 mm ID, 0.25 μm) at 220°C with an isothermal program for 10 min. The initial oven temperature was kept at 50°C for 1 min, then raised to 220°C at 25°C/min and from 200 to 300°C at 8°C/min, and was then maintained for 5.5 min. High purity He (g) was used as the carrier gas at constant flow mode (1.5 ml/min, 45 cm/s linear velocity).

The total phenol was monitored as follows: 40 ml of pharmaceutical industry wastewater was acidified to pH=2.0 by the addition of concentrated HCl. Total phenol was then extracted with ethyl acetate. The organic phase was concentrated at 40°C to about 1 ml and silylized by the addition of N,O-bis(trimethylsilyl) acetamide (BSA). The resulting trimethylsilyl derivatives were analysed by GC-MS (Hewlett-Packard 6980/HP5973MSD).

Methyl tertiary butyl ether (MTBE) was used to extract oil from the water and NPs. GC-MS analysis was performed on an Agilent gas chromatography (GC) system. Oil concentration was measured using a UV–vis spectroscopy fluorescence spectroscopy and a GC–MS (Hewlett-Packard 6980/HP5973MSD). UV–vis absorbance was measured on a UV–vis spectrophotometer and oil concentration was calculated using a calibration plot which was obtained with known oil concentration samples.

Acute Toxicity Assays

Microtox Acute Toxicity Test: Toxicity to the bioluminescent organism *Aliivibrio fischeri (*also called *Vibrio fischeri* or *V. fischeri*) was assayed using the Microtox measuring system according to DIN 38412L34, L341, (EPS 1/ RM/24 1992). Microtox testing was performed according to the standard procedure recommended by the manufacturer (Lange, 1994). A specific strain of the marine bacterium, *V. fischeri*-Microtox LCK 491 kit (Lange, 1994) was used for the Microtox acute toxicity assay. Dr. LANGE LUMIX-mini type luminometer was used for the microtox toxicity assay (Lange, 2010).

***Daphnia magna* Acute Toxicity Test:** To test toxicity, 24-h born *Daphnia magna* were used as described in Standard Methods sections 8711A, 8711B, 8711C, 8711D and 8711E, respectively (Lange, 1996). After preparing the test solution, experiments were carried out using 5 or 10 *Daphnia magna* introduced into the test vessels. These vessels had 100 ml of effective volume at 7.0– 8.0 pH, providing a minimum dissolved oxygen (DO) concentration of 6 mg/l at an ambient temperature of 20–25°C. Young *Daphnia magna* were used in the test (≤24 h old); 24–48 h exposure is generally accepted as standard for a *Daphnia magna* acute toxicity test. The results were expressed as mortality percentage of the *Daphnia magna*. Immobile animals were reported as dead *Daphnia magna*.

Statistical Analysis

ANOVA analysis of variance between experimental data was performed to detect F and *P* values. The ANOVA test was used to test the differences between dependent and independent groups, (Zar, 1984). Comparison between the actual variation of the experimental data averages and standard deviation is expressed in terms of F ratio. F is equal (found variation of the date averages/expected variation of the date averages). *P* reports the significance level, and d.f indicates the number of degrees of freedom. Regression analysis was applied to the experimental data in order to determine the regression coefficient R^2, (Statgraphics Centurion XV, 2005). The aforementioned test was performed using Microsoft Excel Program.

All experiments were carried out three times and the results are given as the means of triplicate samplings. The data relevant to the individual pollutant parameters are given as the mean with standard deviation (SD) values.

Results and Dıscussıons

Electrochemical Filtration Process Mechanism of MWCNT-COOH/BN-NSs/GO Membrane

The electrochemical filtration process mechanism of MWCNT-COOH/BN-NSs/GO membrane was described in Figure 1. Pure GO NPs molecular bonds was shown in Figure 1a. Also, pure BN NPs molecular bonds was demonstrated in Figure 1b. A novel BN-GO NCs molecular bonds structures were indicated in Figure 1c. The electrochemical filtration process mechanism of MWCNT-COOH/BN-NSs/GO membrane between pure GO NPs bonds and pure BN NPs and also -COOH bonds was determined in Figure 1d. The electrochemical filtration process mechanism of MWCNT-COOH/BN-NSs/GO membrane was determined to pure GO NPs: black rectangle, pure BN NPs: grey rectangle and - COOH groups: black line between pure GO NPs and pure BN NPs for CIP removal in pharmaceutical industry wastewater, respectively (Figure 1d).

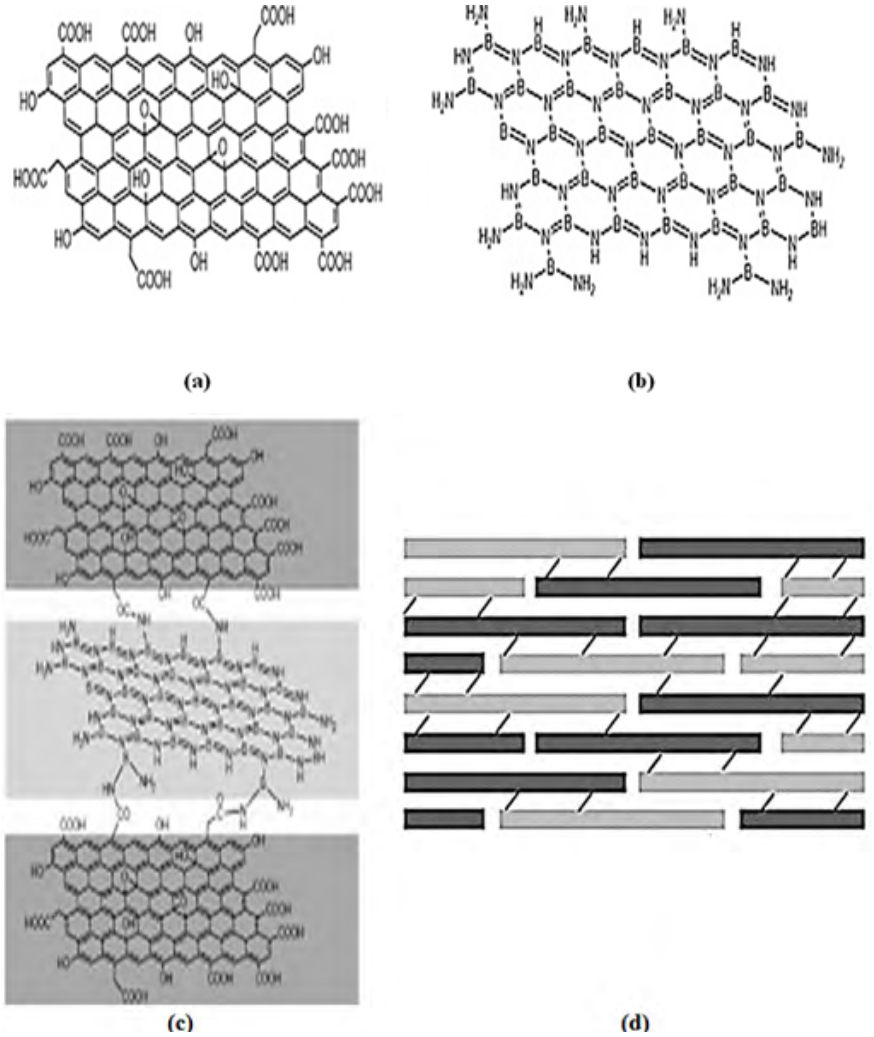

Figure 1: (a) pure GO NPs, (b) pure BN NPs, (c) a novel BN-GO NCs and (d) electrochemical filtration process mechanism of MWCNT-COOH/BN-NSs/GO membrane (pure GO NPs: black rectangle, pure BN NPs: grey rectangle and - COOH groups: black line between pure GO NPs and pure BN NPs) with CIP removal in pharmaceutical industry wastewater, respectively.

MWCNT-COOH/BN nanosheets/GO Membranes Characteristics

The Results of X-Ray Diffraction (XRD) Analysis and Diffuse reflectance UV-Vis Spectra (DRS) Analysis: The results of XRD analysis of as prepared a novel BN-GO NCs with modified at MWCNT-COOH nanotubes (Figure 2a). The characterization peaks were observed at 2θ values of 11.24°, 28.36° and 42.57°, implying pure GO NPs, BN-GO NCs and pure BN NPs in the MWCNT-COOH/BN-NSs/GO membrane (Figure 2a). The XRD patterns of pure GO NPs, a novel BN-GO NCs and pure BN NPs showed the 2θ values of 11.24°, 28.36° and 42.57° corresponding to the (002), (003), and (004) planes of in the MWCNT-COOH/BN-NSs/GO membrane structure, respectively (Figure 2a).

The absorption spectra of CIP was observed in DRS Analysis (Figure 2b). First, the absorption spectra of ciprofloxacin were obtained at a maximum concentration of 200 µg/ml in the wavelength range from 190 nm to 500 nm using diffuse reflectance UV-Vis spectra (Figure 2b). Absorption peaks were observed at wavelengths of 288 nm, 270 nm, 323 nm and 333 nm, respectively (Figure 2b).

The Results of Field Emission Scanning Electron Microscopy (FESEM) and Energy Dispersive X-Ray (EDX) Spectroscopy Analysis: The morphological features of the BN-GO NCs were characterized through FE-SEM images (Figure 3a). In addition to, EDX analysis was also performed to investigate the composition of BN-GO NCs in the MWCNT-COOH/BN-NSs/GO membrane structure (Figure 3b).

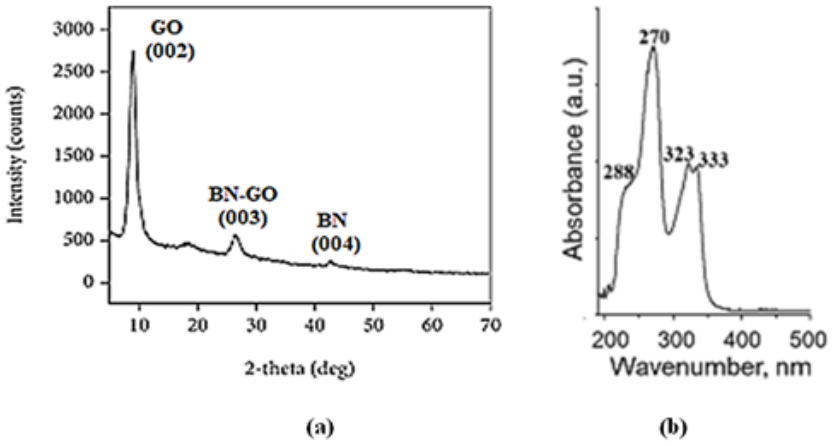

Figure 2: (a) The XRD pattern of pure GO NPs, BN-GO NCs and pure BN NPs in the MWCNT-COOH/BN-NSs/GO membrane structure and (b) the DRS pattern of CIP, respectively.

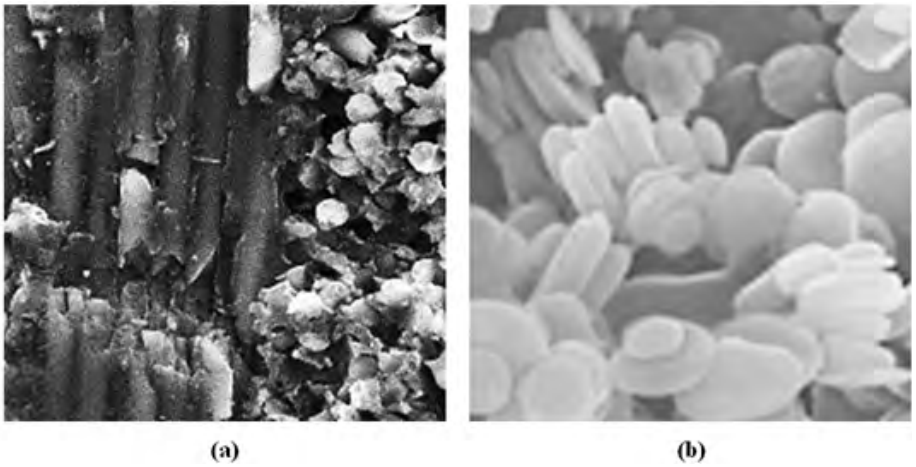

Figure 3: (a) FESEM images of BN-GO NCs and (b) EDX spectrum of BN-GO NCs in the MWCNT-COOH/BN-NSs/GO membrane structure, respectively.

The Results of Fourier Transform Infrared Spectroscopy (FTIR) Analysis and *Transmission Electron Microscopy* (TEM) Analysis: The FTIR spectrum of pure BN NPs (black line), pure GO NPs (red line) and BN-GO NCs (blue line), respectively, in the MWCNT-COOH/BN-NSs/GO membrane (Figure 4a). The main peaks of FTIR spectrum was observed at 3394 1/cm, 1380 1/cm and 806 1/cm wavenumber, respectively (Figure 4a). In addition to, the other peaks of FTIR spectrum was obtained at 1680 1/cm, 1076 1/cm wavenumber, respectively (Figure 4a).

The TEM images of BN-GO NCs in the MWCNT-COOH/BN-NSs/GO membrane structure was observed in micromorphological structure level (Figure 4b).

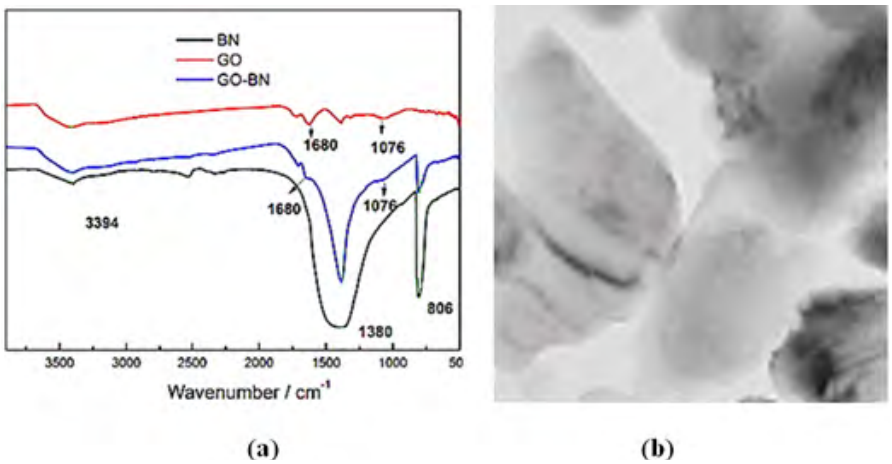

Figure 4: (a) FTIR spectrum of pure BN NPs (black line), pure GO NPs (red line) and BN-GO NCs (blue line) and (b) TEM images of BN-GO NCs in the MWCNT-COOH/BN-NSs/GO membrane structure, respectively.

Effect of Increasing pH values of CIP in the MWCNT/BN-NSs/GO Membrane during Electrochemical Filtration Process in Pharmaceutical Industry Wastewater

Increasing pH values (pH=2.5, pH=3.5, pH=5.5, pH=7.0, pH=9.0 and pH=11.0, respectively) was examined for the removal of CIP in pharmaceutical industry wastewater, at 25°C. CIP removal efficiencies versus increasing pH values was shown with the MWCNT/BN-NSs/GO membrane during electrochemical filtration process in pharmaceutical industry wastewater (Figure 5). 42%, 54%, 63%, 80% and 84% CIP removal efficiencies was measured at pH=2.5, pH=3.5, pH=5.5, pH=7.0 and pH=11.0, respectively, at 25°C (Figure 5). The maximum 97% CIP removal efficiency was obtained with the MWCNT/BN-NSs/GO membrane during electrochemical filtration process in pharmaceutical industry wastewater, at pH=9.0 and at 25°C, respectively (Figure 5).

Effect of Increasing CIP Concentrations in the MWCNT/BN-NSs/GO Membrane during Electrochemical Filtration Process in Pharmaceutical Industry Wastewater

Increasing CIP concentrations (5 mg/l, 15 mg/l, 45 mg/l and 60 mg/l) were operated at pH=9.0, at 25°C, respectively (Figure 6). 82%, 74% and 65% CIP removal efficiencies were obtained to 15 mg/l, 45 mg/l and 60 mg/l CIP concentrations, respectively, at pH=9.0 and at 25°C (Figure 6). The maximum 99% CIP removal efficieny was found with the MWCNT/BN-NSs/GO membrane during electrochemical filtration process in pharmaceutical industry wastewater, at 5 mg/l CIP, at pH=9.0 and at 25°C, respectively (Figure 6).

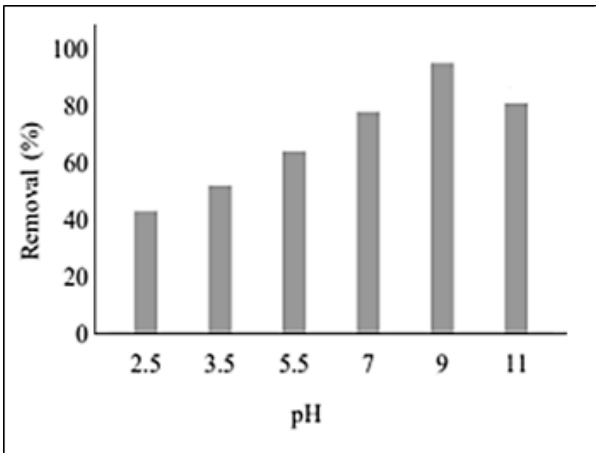

Figure 5: Effect of increasing pH values of CIP in the MWCNT/BN-NSs/GO membrane with electrochemical filtration process in pharmaceutical industry wastewater

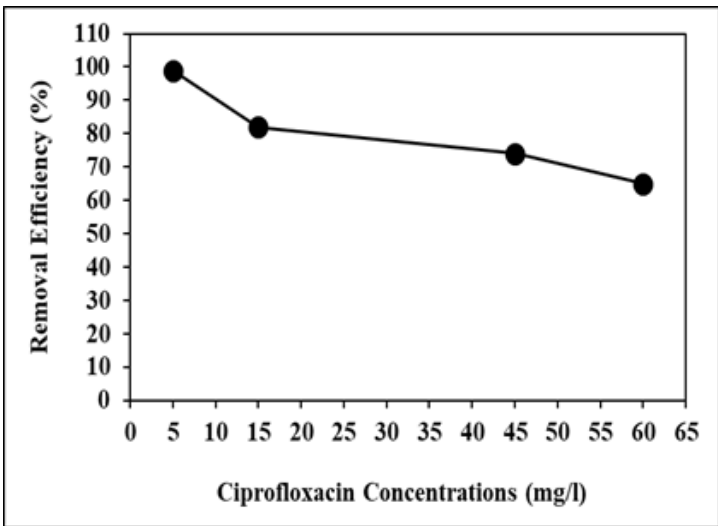

Figure 6: Effect of increasing CIP concentrations in the MWCNT/BN-NSs/GO membrane during electrochemical filtration process in pharmaceutical industry wastewater, at pH=9.0 and at 25oC, respectively.

Effect of Different GO/BN NCs Mass Ratios for the Efficient CIP Removals in the MWCNT/BN-NSs/GO Membrane during Electrochemical Filtration Process in Pharmaceutical Industry Wastewater

Different GO/BN NCs mass ratios (8/1, 4/1, 2/1, 1/1, 1/2, 1/4, 1/8) were examined for the efficient CIP removals in the MWCNT/BN-NSs/GO membrane during electrochemical filtration process in pharmaceutical industry wastewater, at 5 mg/l CIP, at pH=9.0 and at 25°C, respectively (Figure 7). 65%, 74%, 86%, 92%, 80%, 52% CIP removal efficiencies were measured at 8/1, 4/1, 2/1, 1/1, 1/4, 1/8 GO/BN NCs mass ratios, respectively, at 5 mg/l CIP, at pH=9.0 and at 25°C, respectively (Figure 7). The maximum 99% CIP removal efficiency was obtained with the MWCNT/BN-NSs/GO membrane during electrochemical filtration process in pharmaceutical industry wastewater, at 1/2 GO/BN NCs mass ratio, at 5 mg/l CIP, at pH=9.0 and at 25°C, respectively (Figure 7).

Effect of Different Recycle Times for the Efficient CIP Removals in the MWCNT/BN-NSs/GO Membrane during Electrochemical Filtration Process in Pharmaceutical Industry Wastewater

Different recycle times (1, 2, 3, 4, 5, 6 and 7) were operated for the efficient CIP removals in the MWCNT/BN-NSs/GO membrane during electrochemical filtration process in pharmaceutical industry wastewater, at 5 mg/l CIP, at pH=9.0 and at 25°C, respectively (Figure 8). 96%, 90%, 88%, 83%, 80%, 75% CIP removal efficiencies were measured after 2. recycle time, 3. recycle time, 4. recycle time, 5. recycle time, 6. recycle time and 7. recycle time, respectively, at 5 mg/l CIP, at 1/2 GO/BN NCs mass ratio, at pH=9.0 and at 25°C, respectively (Figure 8). The maximum 99% CIP removal efficiency was obtained with the MWCNT/BN-NSs/GO membrane during electrochemical filtration process in pharmaceutical industry wastewater, after 1. recycle time, at 5 mg/l CIP, at pH=9.0 and at 25°C, respectively (Figure 8).

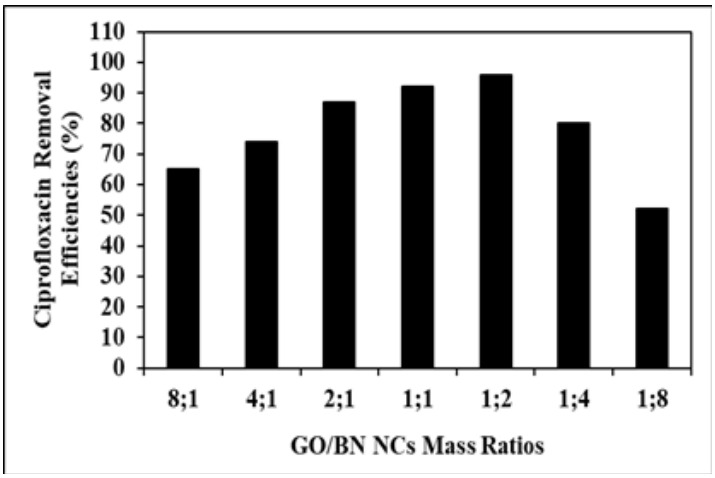

Figure 7: Effect of different GO/BN NCs mass ratios for the efficient CIP removals in the MWCNT/BN-NSs/GO membrane during electrochemical filtration process in pharmaceutical industry wastewater, at 5 mg/l CIP, at pH=9.0 and at 25oC, respectively.

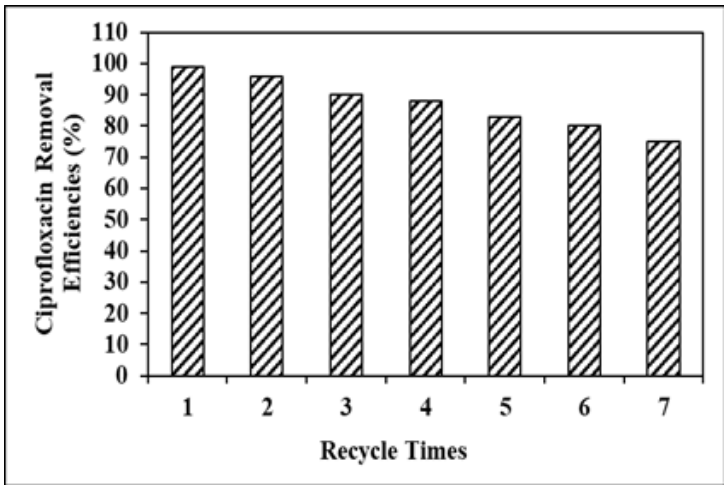

Figure 8: Effect of recycle times for the efficient CIP removals in the MWCNT/BN-NSs/GO membrane during electrochemical filtration process in pharmaceutical industry wastewater, at 5 mg/l CIP, at 1/2 GO/BN NCs mass ratio, at pH=9.0 and at 25oC, respectively.

Acute Toxicity Assays

Effect of Increasing CIP Concentrations on the Microtox Acute Toxicity Removal Efficiencies in Pharmaceutical Industry Wastewater at Increasing Electrochemical Filtration Time and Temperature: In Microtox with *Aliivibrio fischeri* (also called *Vibrio fischeri*) acute toxicity test, the initial EC_{90} values at pH=7.0 was found as 825 mg/l at 25°C (Table 2: SET 1). After 60 min, 120 min and 150 min electrochemical filtration time, the EC_{90} values decreased to EC_{55}=414 mg/l to EC_{20}=236 mg/l and to EC_{10}=165 mg/l in CIP=45 mg/l at 30°C (Table 2: SET 3). The Microtox acute toxicity removal efficiencies were 38.89%, 77.78% and 88.89% after 60 min, 120 min and 150 min, respectively, in CIP=45 mg/l and at 30°C (Table 2: SET 3).

The EC_{90} values decreased to EC_{50}, to EC_{15} and to EC_5 after 60 min, 120 min and 150 min, respectively, in CIP=45 mg/l at 60°C (Table 2: SET 3). The EC_{50}, the EC_{15} and the EC_5 values were measured as 550 mg/l, 540 mg/l and 500 mg/l, respectively, in CIP=45 mg/l at 60°C. The toxicity removal efficiencies were 44.44%, 83.33% and 94.44% after 60 min, 120 min and 150 min, respectively, in CIP=45 mg/l at 60°C (Table 2: SET 3). 94.44% maximum Microtox acute toxicity removal yield was found in CIP=45 mg/l after 150 min and at 60°C (Table 2: SET 3).

The EC_{90} values decreased to EC_{60}=422 mg/l to EC_{25}=241 mg/l and to EC_{15}=168 mg/l after 60 min, 120 min and 150 min, respectively, in CIP=5 mg/l at 30°C (Table 2: SET 3). The EC_{90} values decreased to EC_{60}=421 mg/l to EC_{25}=239 mg/l and to EC_{15}=167 mg/l after 60 min, 120 min and 150 min, respectively, in CIP=15 mg/l at 30°C. The EC_{90} values decreased to EC_{65}=408 mg/l to EC_{30}=230 mg/l and to EC_{20}=162 mg/l after 60 min, 120 min and 150 min, respectively, in CIP=60 mg/l at 30°C. The Microtox acute toxicity removals were 83.33%, 83.33% and 77.78% in 5 mg/l, 15 mg/l and 60 mg/l CIP, respectively, after 150 min, at 30°C. It was obtained an inhibition effect of CIP=60 mg/l to *Vibrio fischeri* after 150 min and at 30°C (Table 2: SET 3).

The EC_{90} values decreased to EC_{55}=419 mg/l to EC_{20}=266 mg/l and to EC_{10}=150 mg/l after 60 min, 120 min and 150 min, respectively, in CIP=5 mg/l at 60°C (Table 2: SET 3). The EC_{90} values decreased to EC_{55}=414 mg/l to EC_{20}=232 mg/l and to EC_{10}=161 mg/l after 60 min, 120 and 150 min, respectively, in CIP=15 mg/l at 60°C. The EC_{90} values decreased to EC_{60}=403 mg/l to EC_{25}=218 mg/l and to EC_{15}=148 mg/l after 60 min, 120 and 150 min, respectively, in CIP=60 mg/l at 60°C. The Microtox acute toxicity removals were 88.89%, 88.89% and 83.33% in 5 mg/l, 15 mg/l and 60 mg/l CIP, respectively, after 150 min, at 60°C. It was observed an inhibition effect of CIP=60 mg/l to Microtox with *Vibrio fischeri* after 150 min, and at 60°C (Table 2: SET 3).

Table 2: Effect of increasing CIP concentrations on Microtox acute toxicity in pharmaceutical industry wastewater after electrochemical filtration process, at 30°C and at 60°C, respectively.

No	Parameters	Microtox Acute Toxicity Values, * EC (mg/l)							
		25°C							
		0 min		60 min		120 min		150 min	
		*EC_{90}		*EC		*EC		*EC	
1	Raw ww, control	825		EC_{70}=510		EC_{60}=650		EC_{50}=640	
		30°C				60°C			
		0. min	60 min	120. min	150. min	0 min	60 min	120 min	150 min
		*EC_{90}	*EC	*EC	*EC	*EC_{90}	*EC	*EC	*EC
2	Raw ww, control	825	EC_{70}= 580	EC_{50}= 580	EC_{40}= 550	825	EC_{55}= 550	EC_{40}= 590	EC_{30}=690
3	CIP=5 mg/l	825	EC_{60}=422	EC_{25}=241	EC_{15}=168	825	EC_{55}=419	EC_{20}=266	EC_{10}=150
	CIP=15 mg/l	825	EC_{60}=421	EC_{25}=239	EC_{15}=167	825	EC_{55}=414	EC_{20}=232	EC_{10}=161
	CIP=45 mg/l	825	EC_{55} =414	EC_{20}=236	EC_{10}=165	825	EC_{50}=550	EC_{15}=540	EC_5=500
	CIP=60 mg/l	825	EC_{65}=408	EC_{30}=230	EC_{20}=162	825	EC_{60}=403	EC_{25}=218	EC_{15}=148

* EC values were calculated based on COD_{dis} (mg/l).

Effect of Increasing CIP Concentrations on the *Daphnia magna* Acute Toxicity Removal Efficiencies in Pharmaceutical Industry Wastewater at Increasing Electrochemical Filtration Time and Temperature

The initial EC_{50} values were observed as 850 mg/l at 25°C (Table 3: SET 1). After 60 min, 120 and 150 min electrochemical filtration time, the EC_{50} values decreased to EC_{30}=350 mg/l to EC_{15}=240 mg/l and to EC_{10}=90 mg/l in CIP=45 mg/l, at 30°C (Table 3: SET 3). The toxicity removal efficiencies were 40%, 70% and 80% after 60 min, 120 min and 150 min, respectively, in CIP=45 mg/l at 30°C (Table 3: SET 3).

The EC_{50} values decreased to EC_{25} to EC_{10} and to EC_5 after 60 min, 120 min and 150 min, respectively, in CIP=45 mg/l at 60°C (Table 3: SET 3). The EC_{25}, the EC_{10} and the EC_5 values were measured

as 150 mg/l, 60 mg/l and 375 mg/l, respectively, in CIP=45 mg/l at 60°C. The toxicity removal efficiencies were 50%, 80% and 90% after 60 min, 120 min and 150 min, respectively, in CIP=45 mg/l at 60°C (Table 3: SET 3). 90% maximum *Daphnia magna* acute toxicity removal was obtained in CIP=45 mg/l after 150 min and at 60°C, respectively (Table 3: SET 3).

The EC_{50} values decreased to EC_{35}=450 mg/l to EC_{20}=145 mg/l and to EC_{15}=260 mg/l after 60 min, 120 min and 150 min, respectively, in CIP=5 mg/l at 30°C (Table 3: SET 3). The EC_{50} values decreased to EC_{35}=450 mg/l to EC_{20}=175 mg/l and to EC_{15}=100 mg/l after 60 min, 120 min and 150 min, respectively, in CIP=15 mg/l and at 30°C. The EC_{50} values decreased to EC_{40}=300 mg/l to EC_{25}=170 mg/l and to EC_{20}=52 mg/l after 60 min, 120 min and 150 min, respectively, in CIP=60 mg/l and at 30°C. The *Daphnia magna* acute toxicity removals were 70%, 70% and 60% in 5 mg/l, 15 mg/l and 60 mg/l CIP, respectively, after 150 min and at 30°C. It was observed an inhibition effect of CIP=60 mg/l to *Daphnia magna* after 150 min and at 30°C (Table 3: SET 3).

The EC_{50} values decreased to EC_{30}=130 mg/l to EC_{15}=425 mg/l and to EC_{10}=340 mg/l after 60 min, 120 min and 150 min, respectively, in CIP=5 mg/l and at 60°C (Table 3: SET 3). The EC_{50} values decreased to EC_{30}=425 mg/l to EC_{15}=140 mg/l and to EC_{5}=90 mg/l after 60 min, 120 min and 150 min, respectively, in CIP=15 mg/l and at 60°C. The EC_{50} values decreased to EC_{35}=250 mg/l to EC_{20}=110 mg/l and to EC_{15}=11 mg/l after 60 min, 120 min and 150 min, respectively, in CIP=60 mg/l and at 60°C. The *Daphnia magna* acute toxicity removals were 80%, 90% and 70% in 5 mg/l, 15 mg/l and 60 mg/l CIP, respectively, after 150 min and at 60°C. It was observed an inhibition effect of CIP=60 mg/l to *Daphnia magna* after 150 min and at 60°C (Table 3: SET 3).

Increasing the CIP concentrations from 5 mg/l to 60 mg/l did not have a positive effect on the decrease of EC_{50} values as shown in Table 3 at SET 3. CIP concentrations > 45 mg/l decreased the acute toxicity removals by hindering the electrochemical filtration process. Similarly, a significant contribution of increasing CIP concentration to acute toxicity removal at 60°C after 150 min of electrochemical filtration time was not observed. Low toxicity removals found at high CIP concentrations could be attributed to their detrimental effect on the *Daphnia magna* (Table 3: SET 3).

Table 3: Effect of increasing CIP concentrations on *Daphnia magna* acute toxicity in pharmaceutical industry wastewater after electrochemical filtration process, at 30°C and at 60°C.

No	Parameters	***Daphnia magna* Acute Toxicity Values, * EC (mg/l)**							
		25°C							
		0. min		**60. min**		**120. min**		**150. min**	
		***EC_{50}**		***EC**		***EC**		***EC**	
1	Raw ww, control	850		EC_{45}=625		EC_{40}=370		EC_{30}=155	
		30°C				**60°C**			
		0 min	**60 min**	**120 min**	**150. min**	**0. min**	**60. min**	**120. min**	**150. min**
		***EC_{50}**	***EC**	***EC**	***EC**	***EC_{50}**	***EC**	***EC**	***EC**
2	Raw ww, control	850	EC_{40}=470	EC_{35}=230	EC_{25}=115	850	EC_{35}=375	EC_{30}=212	EC_{20}=75
3	CIP=5 mg/l	850	EC_{35}=450	EC_{20}=145	EC_{15}=260	850	EC_{30}=130	EC_{15}=425	EC_{10}=340
	CIP=15 mg/l	850	EC_{35}=450	EC_{20}=175	EC_{15}=100	850	EC_{30}=425	EC_{15}=140	EC_{5}=90
	CIP=45 mg/l	850	EC_{30}=350	EC_{15}=240	EC_{10}=90	850	EC_{25}=150	EC_{10}=60	EC_{5}=375
	CIP=60 mg/l	850	EC_{40}=300	EC_{25}=170	EC_{20}=52	850	EC_{35}=250	EC_{20}=110	EC_{15}=11

* EC values were calculated based on COD_{dis} (mg/l).

Direct Effects of CIP Concentrations on the Acute Toxicity of Microtox and *Daphnia magna* without Pharmaceutical Industry Wastewater after Electrochemical Filtration Process: The acute toxicity test was performed in the samples containing 5 mg/l, 15 mg/l, 45 mg/l and 60 mg/l CIP concentrations. In order to detect the direct responses of Microtox and *Daphnia magna* to the increasing CIP concentrations the toxicity test were performed without pharmaceutical industry wastewater after electrochemical filtration process. The initial EC values and the the EC_{50} values were measured in the samples containing increasing CIP concentrations after 150 min electrochemical filtration time. Table 4 showed the responses of Microtox and *Daphnia magna* to increasing CIP concentrations.

The acute toxicity originating only from 5 mg/l, 15 mg/l, 45 mg/l and 60 mg/l CIP were found to be low (Table 4). 5 mg/l CIP did not exhibited toxicity to *Vibrio fischeri* and *Daphnia magna* before and after 150 min electrochemical filtration time. The toxicity atributed to the 15 mg/l, 45 mg/l and 60 mg/l CIP were found to be low in the samples without pharmaceutical industry wastewater after electrochemical filtration process for the test organisms mentioned above. The acute toxicity originated from the CIP decreased

significantly to EC_1, EC_4 and EC_6 after 150 min electrochemical filtration time. Therefore, it can be concluded that the toxicity originating from the CIP is not significant and the real acute toxicity throughout electrochemical filtration process was attributed to the pharmaceutical industry wastewater, to their metabolites and to the electrochemical filtration by-products (Table 4).

The maximum 97% CIP removal efficiency was obtained with the MWCNT/BN-NSs/GO membrane during electrochemical filtration process in pharmaceutical industry wastewater, at pH=9.0 and at 25°C, respectively.

The maximum 99% CIP removal efficieny was found with the MWCNT/BN-NSs/GO membrane during electrochemical filtration process in pharmaceutical industry wastewater, at 5 mg/l CIP, at pH=9.0 and at 25°C, respectively.

Table 4: The responses of Microtox and Daphnia magna acute toxicity tests in addition of increasing CIP concentrations without phamaceutical industry wastewater during electrochemical filtration process after 150 min electrochemical filtration time.

	Microtox Acute Toxicity Test			*Daphnia magna* Acute Toxicity Test		
CIP Conc. (mg/l)	**Initial Acute Toxicity EC_{50} Value (mg/l)**	**Inhibitions after 150 min electrochemical filtration**	**EC Values (mg/l)**	**Initial Acute Toxicity EC_{50} Value (mg/l)**	**Inhibitions after 150 min electrochemical filtration**	**EC Values (mg/l)**
5	EC_{10}=25	-	-	EC_{10}=40	-	-
15	EC_{15}=80	4	EC_1=4	EC_{20}=100	6	EC_3=6
45	EC_{20}=150	6	EC_4=7	EC_{30}=200	7	EC_6=12
60	EC_{25}=220	8	EC_6=10	EC_{40}=300	10	EC_8=16

Conclusıons

The maximum 99% CIP removal efficiency was obtained with the MWCNT/BN-NSs/GO membrane during electrochemical filtration prcoess in pharmaceutical industry wastewater, at 1/2 GO/BN NCs mass ratio, at 5 mg/l CIP, at pH=9.0 and at 25°C, respectively.

The maximum 99% CIP removal efficiency was obtained with the MWCNT/BN-NSs/GO membrane during electrochemical filtration process in pharmaceutical industry wastewater, after 1. recycle time, at 5 mg/l CIP, at pH=9.0 and at 25°C, respectively.

94.44% maximum Microtox acute toxicity yield was found in CIP=45 mg/l after 150 min electrochemical filtration time and at 60°C, respectively. It was observed an inhibition effect of CIP=60 mg/l to Microtox with *Vibrio fischeri* after 150 min electrochemical filtration time at 60°C. 90% maximum *Daphnia magna* acute toxicity removal was obtained in CIP=45 mg/l after 150 min electrochemical filtration time and at 60°C, respectively. It was observed an inhibition effect of CIP=60 mg/l to *Daphnia magna* after 150 min electrochemical filtration time and at 60°C. CIP concentrations > 45 mg/l decreased the acute toxicity removals by hindering the electrochemical filtration process. Similarly, a significant contribution of increasing CIP concentrations to acute toxicity removal at 60°C after 150 min electrochemical filtration time was not observed. Finally, it can be concluded that the toxicity originating from the CIP is not significant and the real acute toxicity throughout electrochemical filtration process was attributed to the pharmaceutical industry wastewater, to their metabolites and to the electrochemical filtration by-products.

As a result, the MWCNT/BN-NSs/GO membrane during electrochemical filtration process in pharmaceutical industry wastewater was stable in harsh environments such as acidic, alkaline, saline, and then was still effective process. When the amount of contaminant was increased, the the MWCNT/BN-NSs/GO membrane performance was still considerable. Finally, the combination of a simple, easy operation preparation process and excellent performance makes this MWCNT/BN-NSs/GO membrane a promising option during electrochemical fitration process in pharmaceutical industry wastewater treatment.

Acknowledgement

This research study was undertaken in the Environmental Microbiology Laboratories at Dokuz Eylül University Engineering Faculty Environmental Engineering Department, Izmir, Turkey. The authors would like to thank this body for providing financial support.

References

1. Abdikheibari S, Lei W, Dumee LF, Milne N, Baskaran K. Thin film nanocomposite nanofiltration membranes from amine functionalized-boron nitride/polypiperazine amide with enhanced flux and fouling resistance. J. Mater. Chem. A. 2018; 6: 12066–12081.
2. Ahammad NA, Zulkifli MA, Ahmad MA, Hameed BH, Mohd Din AT. Desorption of chloramphenicol from ordered mesoporous carbonalginate beads: Effects of operating parameters, and isotherm, kinetics, and regeneration studies. J. Environ. Chem. Eng. 2021;9: 105015.
3. Ahmed MB, Zhou JL, Ngo HH, Guo W. Adsorptive removal of antibiotics from water and wastewater: Progress and challenges. Sci. Total Environ. 2015; 532: 112–126.
4. Ahmed MB, Zhou J, Ngo HH, Guo W, Johir MAH, Sornalingam K, et al. Nano-Fe0 immobilized onto functionalized biochar gaining excellent stability during sorption and reduction of chloramphenı-

col via transforming to reusable magnetic composite. Chem. Eng. J. 2017; 322:571–581.

5. Akyon B, McLaughlin M, Hernández F, Blotevogel J, Bibby K. Characterization and biological removal of organic compounds from hydraulic fracturing produced water. Environ. Sci. Process. 2019; 21:279–290.
6. Alagha O, Ouerfelli N, Kochkar H, Almessiere MA, Slimani Y, Manikandan A, et al. Kinetic modeling for photo-assisted penicillin G degradation of (Mn0.5Zn0.5)[CdxFe2-x]O4 ($x \leq 0.05$) nanospinel ferrites. Nanomaterials. 2021; 11; 970-986.
7. ALOthman ZA, Badjah AY, Alharbi OML, Ali I. Synthesis of chitosan composite iron nanoparticles for removal of diclofenac sodium drug residue in water. Int. J. Biol. Macromol. 2020; 159: 870–876.
8. Alygizakis NA, Gago-Ferrero P, Borova VL, Pavlidou A, Hatzianestis I, Thomaidis NS, et al. Occurrence and spatial distribution of 158 pharmaceuticals, drugs of abuse and related metabolites in offshore seawater. Sci. Total Environ. 2016; 541: 1097–1105.
9. Arenas NE, Melo VM. Producción pecuaria y emergencia de antibiótico resistencia en Colombia: Revisión sistemática. Infectio. 2018; 22: 110–119.
10. Avcu T, Üner O, Geçgel Ü. Adsorptive removal of diclofenac sodium from aqueous solution onto sycamore ball activated carbon – isotherms, kinetics, and thermodynamic study, Surfaces and Interfaces. 2021; 24: 101097.
11. Baird RB, Eaton AD, Rice EW. Standard Methods for the Examination of Water and Wastewater. 23rd. Edition, Rice, E.W. (editors), American Public Health Association (APHA), American Water Works Association (AWWA), Water Environment Federation (WEF). American Public Health Association 800 I Street, NW Washington DC: 20001-3770, USA, January 1, 2017; ISBN-13: 978-0875532875; ISBN-10: 087553287X.
12. Bansod B, Kumar T, Thakur R, Rana S, Singh I. A review on various electrochemical techniques for heavy metal ions detection with different sensing platforms, Biosens. Bioelectron. 2017; 94: 443–455.
13. Bao J, Zhu Y, Yuan S, Wang F, Tang H, Bao Z, et al. Adsorption of tetracycline with reduced graphene oxide decorated with MnFe2O4 nanoparticles. Nanoscale Res. Lett. 2018; 13: 396-403.
14. Barry S. Dangerously high levels of antibiotics found in world's major rivers, says study, World news global study. Euronews. 2019; 1: 1-10.
15. Bellamkonda S, Thangavel N, Hafeez HY, Neppolian B, Ranga Rao G. Highly active and stable multi-walled carbon nanotubes-graphene-TiO2 nanohybrid: An efficient non-noble metal photocatalyst for water splitting, Catal. Today. 2019; 321(322): 120–127.
16. Casanova LM, Sobsey MD. Antibiotic-resistant enteric bacteria in environmental waters. Water. 2016; 8(12): 561-567.
17. Cheng C, Jiang G, Garvey CJ, Wang Y, Simon GP, Liu JZ, et al. Ion transport in complex layered graphene-based membranes with tuneable interlayer spacing. Sci. Adv. 2016; 2(2): e1501272.
18. Cohen-Tanugi D, Grossman JC. Water desalination across nanoporous graphene. Nano Lett. 2012; 12: 3602–3608.
19. Cui G, Guo J, Zhang Y, Zhao Q, Fu S, Han T, et al. Chitosan oligosaccharide derivatives as green corrosion inhibitors for P110 steel in a carbon-dioxide-saturated chloride solution. Carbohydr. Polym. 2019; 203: 386–395.
20. Dai P, Xue Y, Wang X, Weng Q, Zhang C, Jiang X, et al. Pollutant capturing SERS substrate: porous boron nitride microfibers with uniform silver nanoparticle decoration. Nanoscale. 2015; 7: 18992–18997.
21. De Souza Santos LV, Meireles AM, Lange LC. Degradation of antibiotics norfloxacin by fenton, UV and UV/H2O2. J. Environ. Manag. 2015; 154: 8–12.
22. Dehghan A, Mohammadi AA, Yousefi M, Najafpoor AA, Shams M, Rezania S, et al. Enhanced kinetic removal of ciprofloxacin onto metal-organic frameworks by sonication, process optimization and metal leaching study. Nanomaterials. 2019; 9(10): 1422-1438.
23. Dinh QT, Moreau-Guigon E, Labadie P, Alliot F, Teil MJ, Blanchard M, et al. Occurrence of antibiotics in rural catchments. Chemosphere. 2017; 168: 483–490.
24. Dong D, Zhang L, Liu S, Guo Z, Hua X. Antibiotics in Water and Sediments from Liao River in Jilin Province, China: occurrence, distribution, and risk assessment. Environ. Earth Sci. 2016; 75(16): 1202.
25. Eckenfelder WW. Industrial Water Pollution Control (2nd ed), Signapore: McGraw-Hill Inc. 1989.
26. Falin A, Cai Q, Santos EJG, Scullion D, Qian D, Zhang R, et al. Mechanical properties of atomically thin boron nitride and the role of interlayer interactions. Nat. Commun. 2017; 8(9): 15815-15823.
27. Falyouna O, Idham MF, Maamoun I, Bensaida K, Ashik UPM, Sugihara Y, et al. Promotion of ciprofloxacin adsorption from contaminated solutions by oxalate modified nanoscale zerovalent iron particles. J. Mol. Liq. 2022; 359: 119323.
28. Falyouna O, Maamoun I, Bensaida K, Tahara A, Sugihara Y, Eljamal O, et al. Encapsulation of iron nanoparticles with magnesium hydroxide shell for remarkable removal of ciprofloxacin from contaminated water. J. Colloid Interface Sci. 2022; 605: 813-827.
29. Fan Y, Yang Z, Hua WX, Liu D, Tao T, Rahman MM, et al. Functionalized boron nitride nanosheets/graphene ınterlayer for fast and long-life lithium-sulfur batteries. Adv. Energy Mater. 2017; 7(13): 1602380: 1-6.
30. Fang H, Oberoi AS, He Z, Khanal SK, Lu H. Ciprofloxacin degrading paraclostridium sp. Isolated from sulfate reducing bacteria-enriched sludge: optimization and mechanism. Water Res. 2021; 191: 116808.
31. Fathizadeh M, Xu WL, Zhou F, Yoon Y, Yu M. Graphene Oxide: A Novel 2-Dimensional material in membrane separation for water purification, Adv. Mater. Interfaces. 2017; 4(5): 1600918.
32. Fekadu S, Alemayehu E, Dewil R, Van der Bruggen B. Pharmaceuticals in freshwater aquatic environments: a comparison of the african and european challenge. Sci. Total Environ. 2019; 654: 324–337.
33. Ferri M, Ranucci E, Romagnoli P, Giaccone V. Antimicrobial resistance: A global emerging threat to public health systems. Crit. Rev.

Food Sci. 2017; 57: 2857–2876.

34. Firouzeh N, Malakootian M, Asadzadeh SN, Khatami M, Makarem Z. Degradation of ciprofloxacin using ultrasound/ZnO/oxone process from aqueous solution lab-scale analysis and optimization. BioNanoScience. 2021; 11(2): 306-313.
35. Fridkin S, Baggs J, Fagan R, Magill S, Pollack LA, Malpiedi P, et al. Vital Signs: Improving Antibiotic Use Among hospitalized patients, MMWR-Morb. Mortal. Wkly. Rep. 2014; 63(9): 194-200.
36. Gonzalez-Ortiz D, Pochat-Bohatier C, Gassara S, Cambedouzou J, Bechelany M, Miele P, et al. Development of novel h-BNNS/PVA porous membranes via pickering emulsion templating, Green Chem. 2018; 20: 4319–4329.
37. Görmez F, Görmez Ö, Gözmen B, Kalderis D. Degradation of chloramphenicol and metronidazole by electro-fenton process using graphene oxideFe3O4 as heterogeneous catalyst. J. Environ. Chem. Eng. 2019; 7: 102990.
38. Gudz KY, Permyakova ES, Matveev AT, Bondarev AV, Manakhov AM, Sidorenko DA, et al. Pristine and antibiotic-loaded nanosheets/nanoneedles-based boron nitride films as a promising platform to suppress bacterial and fungal infections, ACS Appl. Mater. Interfaces. 2020; 12(38): 42485–42498.
39. Gupta B, Kumar Gupta A, Sekhar Tiwary C, Ghosal PS. A multivariate modeling and experimental realization of photocatalytic system of engineered S–C3N4/ZnO hybrid for ciprofloxacin removal: Influencing factors and degradation pathways. Environ Res. 2021; 196: 110390.
40. Hirunpinyopas W, Prestat E, Worrall SD, Haigh SJ, Dryfe RAW, Bissett MA, et al. Desalination and nanofiltration through functionalized laminar MoS2 membranes. ACS Nano. 2017; 11: 11082-11090.
41. Homaeigohar S, Elbahri M. Graphene membranes for water desalination. NPG Asia Mater. 2017; 9: e427.
42. Hummers WS, Offeman RE. Preparation of graphitic oxide, Journal of the American Chemical Society. 1958; 80(6): 1339.
43. Huo TI. The first case of multidrug-resistant NDM−1-harboring Enterobacteriaceae in Taiwan: here comes the superbacteria!. J. Chin. Med. Assoc. 2010; 73: 557–558.
44. Idham MF, Abdullah B, Yusof KM. Effects of two cycle heat treatment on the microstructure and hardness of ductile iron. Pertanika J. Sci. Technol. 2017; 25: 99–106.
45. Idham MF, Falyouna O, Eljamal O. Effect of graphene oxide synthesis method on the adsorption performance of pharmaceutical contaminants. Proc. Int. Exch. Innov. Conf. Eng. Sci. 2021; 7: 232–239.
46. Ji Y, Zhang C, Zhang XJ, Xie PF, Wu C, Jiang L, et al. A high adsorption capacity bamboo biochar for CO2 capture for low temperature heat utilization. Sep. Purif. Technol. 2022; 293: 121131.
47. Jiang Q, Zhang Y, Jiang S, Wang Y, Li H, Han W, et al. Graphene-like carbon sheetsupported nZVI for efficient atrazine oxidation degradation by persulfate activation. Chem. Eng. J. 2020; 403: 126309.
48. Jiao S, Xu Z. Non-continuum ıntercalated water diffusion explains fast permeation through graphene oxide membranes. ACS Nano. 2017; 11: 11152–11161.
49. Jiménez-Tototzintle M, Ferreira IJ, Da Silva Duque S, Guimarães Barrocas PR, Saggioro EM. Removal of contaminants of emerging concern (CECs) and antibiotic resistant bacteria in urban wastewater using UVA/TiO2/H2O2 photocatalysis. Chemosphere. 2018; 210: 449–457.
50. Karthikeyan KG, Meyer MT. Occurrence of antibiotics in wastewater treatment facilities in Wisconsin, USA. Sci. Total Environ. 2006; 361: 196–207.
51. Kaur Sodhi K, Kumar Singh D. Insight into the fluoroquinolone resistance, sources, ecotoxicity, and degradation with special emphasis on ciprofloxacin. J. Water Process. Eng. 2021; 43: 102218.
52. Kerrigan JF, Sandberg KD, Engstrom DR, LaPara TM, Arnold WA. Small and large-scale distribution of four classes of antibiotics in sediment: association with metals and antibiotic resistance genes, Environ. Sci. Process. Impacts. 2018; 20: 1167–1179.
53. Khalil AME, Memon FA, Tabish TA, Salmon D, Zhang S, Butler D, et al. Nanostructured porous graphene for efficient removal of emerging contaminants (pharmaceuticals) from water. Chem. Eng. J. 2020; 398: 125440.
54. Kumunda C, Adekunle SA, Mamba BB, Hlongwa NW, Nkambule TTI. Electrochemical detection of environmental pollutants based on graphene derivatives: A review, Front Mater. 2021; 7: 616787.
55. Lange B. LUMISmini, Operating Manual. Düsseldorf, Germany: Dr Bruno LANGE. 1994.
56. Lange B. LUMIXmini type luminometer. Dusseldorf: Dr LANGE Company. 1996.
57. Lange B. Vibrio fischeri -Microtox LCK 491 kit. Germany: Dr LANGE. 2010.
58. Li H, Hu J, Meng Y, Su J, Wang X. An investigation into the rapid removal of tetracycline using multilayered graphene-phase biochar derived from waste chicken feather. Sci. Total Environ. 2017; 603-604: 39–48.
59. Li Q, Yang T, Yang Q, Wang F, Chou KC, Hou X. Porous hexagonal boron nitride whiskers fabricated at low temperature for effective removal of organic pollutants from water, Ceram. Int. 2016; 42: 8754–8762.
60. Li X, Wang X, Zhang J, Hanagata N, Wang X, Weng Q, et al. Hollow boron nitride nanospheres as boron reservoir for prostate cancer treatment. Nat. Commun. 2017; 8: 13936.
61. Li Y, Gutiérrez Moreno JJ, Song Z, Liu D, Wang M, Ramiere A, et al. Controlled synthesis of perforated oxide nanosheets with high density nanopores showing superior water purification performance, ACS Appl. Mater. Interfaces. 2022; 14: 18513-18524.
62. Liu D, Zhang M, Xie W, Sun L, Chen Y, Lei W. Porous BN/TiO2 hybrid nanosheets as highly efficient visible-light-driven photocatalysts. Appl. Catal. B-Environ. 2017; 207: 72–78.

63. Liu WX, Song S, Ye ML, Zhu Y, Zhao YG, Lu Y, et al. Nanomaterials with excellent adsorption characteristics for sample pretreatment: a review. Nanomaterials. 2022; 12: 1845.
64. Liu YP, Lv YT, Guan JF, Khoso FM, Jiang XY, Chen J, Li WJ, Yu JG. Rational design of three-dimensional graphene/graphene oxide-based architectures for the efficient adsorption of contaminants from aqueous solutions. J. Mol. Liq. 2021; 343: 117709.
65. Maiti K, Thanh TD, Sharma K, Hui D, Kim NH, Lee JH. Highly efficient adsorbent based on novel cotton flower-like porous boron nitride for organic pollutant removal, Compos. Part B Eng. 2017; 123: 45–54.
66. Malakootian M, Nasiri A, Asadipour A, Kargar E. Facile and green synthesis of ZnFe2 O4 @ CMC as a new magnetic nanophotocatalyst for ciprofloxacin degradation from aqueous media, Process Saf Environ Prot. 2019; 129: 138-51.
67. Masoudi F, Kamranifar M, Safari F, Naghizadeh A. Mechanism, kinetics and thermodynamic of Penicillin G antibiotic removal by silica nanoparticles from simulated hospital wastewater, Desalination Water Treat. 2019; 169: 333–341.
68. Maycock DS, Watts CD. Pharmaceuticals in drinking water, Encycl. Environ. Heal. 2011; 472–484.
69. McConnell MM, Truelstrup Hansen L, Jamieson RC, Neudorf KD, Yost CK, Tong A. Removal of antibiotic resistance genes in two tertiary level municipal wastewater treatment plants. Sci. Total Environ. 2018; 643: 292–300.
70. Mi B. Graphene oxide membranes for ionic and molecular sieving, Science. 2014; 343: 740–742.
71. Mokhati A, Benturki O, Bernardo M, Kecira Z, Matos I, Lapa N, et al. Nanoporous carbons prepared from argan nutshells as potential removal agents of diclofenac and paroxetine. J. Mol. Liq. 2021; 326: 115368.
72. Nguyen CH, Tran ML, Van Tran TT, Juang RS. Efficient removal of antibiotic oxytetracycline from water by Fenton-like reactions using reduced graphene oxide-supported bimetallic Pd/nZVI nanocomposites. J. Taiwan Inst. Chem. Eng. 2021; 119: 80–89.
73. Nguyen LT, Nguyen HT, Pham TD, Tran TD, Chu HT, Dang HT, Van Der Bruggen B. UV–visible light driven photocatalytic degradation of ciprofloxacin by N, S co-doped TiO2: the effect of operational parameters, Topics in Catalysis. 2020; 63(11): 985-995.
74. Olthof M, Eckenfelder WW. Coagulation of textile wastewater, Textile, Chemistry and Colorists. 1976; 8: 18-22.
75. Pan L, Liu YT, Xie XM, Ye XY. Facile and green production of ımpurity-free aqueous solutions of WS2 nanosheets by direct exfoliation in water. Small. 2016; 12: 6703–6713.
76. Park HB, Kamcev J, Robeson LM, Elimelech M, Freeman BD. Maximizing the right stuff: The trade-off between membrane permeability and selectivity. Science. 2017; 356(6343): eaab0530
77. Pellerito A, Ameen SM, Micali M, Caruso G. Antimicrobial substances for food packaging products: the current situation. J. AOAC Int. 2018; 101(4): 942-947.
78. Peng W, Li H, Liu Y, Song S. A review on heavy metal ions adsorption from water by graphene oxide and its composites. J. Mol. Liq. 2017; 230: 496-504.
79. Phasuphan W, Praphairaksit N, Imyim A. Removal of ibuprofen, diclofenac, and naproxen from water using chitosan-modified waste tire crumb rubber. J. Mol. Liq. 2019; 294: 111554.
80. Portehault D, Giordano C, Gervais C, Senkovska I, Kaskel S, et al. High-surface-area nanoporous boron carbon nitrides for hydrogen storage. Adv. Funct. Mater. 2010; 20: 1827–1833.
81. Qiao D, Li Z, Duan J, He X. Adsorption and photocatalytic degradation mechanism of magnetic graphene oxide/ZnO nanocomposites for tetracycline contaminants. Chem. Eng. J. 2020; 400: 125952.
82. Razmjou A, Resosudarmo A, Holmes RL, Li H, Mansouri J, Chen V. The effect of modified TiO2 nanoparticles on the polyethersulfone ultrafiltration hollow fiber membranes. Desalination. 2012; 287: 271–280.
83. Rigueto CVT, Rosseto M, Nazari MT, Ostwald BEP, Alessandretti I, Manera C, et al. Adsorption of diclofenac sodium by composite beads prepared from tannery wastesderived gelatin and carbon nanotubes. J. Environ. Chem. Eng. 2021; 9: 105030.
84. Shahnaz T, Vishnu Priyan V, Pandian S, Narayanasamy S. Use of nanocellulose extracted from grass for adsorption abatement of Ciprofloxacin and Diclofenac removal with phyto, and fish toxicity studies. Environ. Pollut. 2021; 268: 115494.
85. Shan D, Deng S, Li J, Wang H, He C, Cagnetta G, Wang B, Wang Y, Huang J, Yu G. Preparation of porous graphene oxide by chemically intercalating a rigid molecule for enhanced removal of typical pharmaceuticals. Carbon NY. 2017; 119: 101–109.
86. Shi J, Tong R, Zhou X, Gong Y, Zhang Z, Ji Q, et al. Temperature-mediated selective growth of MoS2/WS2 and WS2/MoS2 vertical stacks on Au foils for direct photocatalytic applications. Adv. Mater. 2016; 28(48): 10664-10672.
87. Shirani Z, Song H, Bhatnagar A. Efficient removal of diclofenac and cephalexin from aqueous solution using Anthriscus sylvestris-derived activated biochar. Sci. Total Environ. 2020; 745: 140789.
88. Siedlewicz G, Białk-Bielinska A, Borecka M, Winogradow A, Stepnowski P, Pazdro K. Presence, concentrations and risk assessment of selected antibiotic residues in sediments and near-bottom waters collected from the Polish Coastal Zone in the Southern Baltic Sea—Summary of 3years of studies, Mar. Pollut. Bull. 2018; 129: 787–801.
89. Silwana B, Van Der Horst C, Iwuoha E, Somerset V. A brief review on recent developments of electrochemical sensors in environmental application for PGMs, J. Environ. Sci. Health A Tox. Hazard Subst. Environ. Eng. 2016; 51: 1233–1247.
90. Smith AT, Anna MLC, Songshan Z, Bin L, Luyi S. Synthesis, properties, and applications of graphene oxide/reduced graphene oxide and their nanocomposites. Nano Mater. Sci. 2019; 1: 31–47.
91. Statgraphics Centurion XV, sofware, StatPoint Inc, Statgraphics Centurion XV, Herndon, VA, USA, 2005.

92. Sturini M, Puscalau C, Guerra G, Maraschi F, Bruni G, Monteforte F, et al. Combined layer-by-layer/hydrothermal synthesis of Fe3O4@ MIL-100(Fe) for ofloxacin adsorption from environmental waters. Nanomaterials. 2021; 11: 3275.

93. Sun T, Fan R, Zhang J, Qin M, Chen W, Jiang X, et al. Stimuli-Responsive metal–organic framework on a metal–organic framework heterostructure for efficient antibiotic detection and anticounterfeiting, ACS Appl. Mater. Interfaces. 2021; 13: 35689-99.

94. Swapna Priya S, Radha KV. A review on the adsorption studies of tetracycline onto various types of adsorbents, Chem. Eng. Commun. 2017; 204: 821–839.

95. Tamaddon F, Nasiri A, Yazdanpanah G. Photocatalytic degradation of ciprofloxacin using CuFe2 O4 @ methyl cellulose based magnetic nanobiocomposite. MethodsX. 2020; 7:100764.

96. Tamma PD, Avdic E, Li DX, Dzintars K, Cosgrove SE. Association of adverse events with antibiotic use in hospitalized patients. JAMA Intern. Med. 2017; 177: 1308-15.

97. Tan L, Li LY, Ashbolt N, Wang XL, Cui YX, Zhu X, et al. Arctic antibiotic resistance gene contamination, a result of anthropogenic activities and natural origin. Sci. Total Environ. 2018; 621: 1176-84.

98. Tang C, Bando Y, Shen G, Zhi C, Golberg D. Single-source precursor for chemical vapour deposition of collapsed boron nitride nanotubes. Nanotechnology. 2006; 17: 5882–5888.

99. Tang H, Li W, Jiang H, Lin R, Wang Z, Wu J, He G, Shearing PR, Brett DJL. ZIF-8-derived hollow carbon for efficient adsorption of antibiotics. Nanomaterials. 2019; 9: 117.

100. Tang X, Wang Z, Wang Y. Visible active N-doped TiO2/reduced graphene oxide for the degradation of tetracycline hydrochloride. Chem. Phys. Lett. 2018; 691: 408–414.

101. Teodosiu C, Gilca AF, Barjoveanu G, Fiore S. Emerging pollutants removal through advanced drinking water treatment: A review on processes and environmental performances assessment. J. Clean. Prod. 2018; 197: 1210-21.

102. Tong S, Pan J, Lu S, Tang J. Patient compliance with antimicrobial drugs: A Chinese survey, Am. J. Infect. Control. 2018; 46: E25-E29.

103. Wang J, Hao J, Liu D, Qin S, Chen C, Yang C, Liu Y, Yang T, Fan Y, Chen Y, Lei W. Flower stamen-like porous boron carbon nitride nanoscrolls for water cleaning. Nanoscale. 2017a; 9: 9787–9791.

104. Wang X, Wang A, Lu M, Ma J. Synthesis of magnetically recoverable Fe0/graphene-TiO2 nanowires composite for both reduction and photocatalytic oxidation of metronidazole. Chem. Eng. J. 2017b; 337: 372–384.

105. Wang X, Yin R, Zeng L, Zhu M. A Review of graphene-based nanomaterials for removal of antibiotics from aqueous environments, Environ. Pollut. 2019; 253: 100–110.

106. Wang Z, Song L, Wang Y, Zhang XF, Yao J. Construction of a hybrid graphene oxide/nanofibrillated cellulose aerogel used for the efficient removal of methylene blue and tetracycline. J. Phys. Chem. Solids. 2021; 150: 109839.

107. Wong A, Scontri M, Materon EM, Lanza MRV, Sotomayor MDPT. Development and application of an electrochemical sensor modified with multi-walled carbon nanotubes and graphene oxide for the sensitive and selective detection of tetracycline. J. Electroanal. Chem. 2015; 757: 250–257.

108. Xue L, Lu B, Wu ZS, Ge C, Wang P, Zhang R, Zhang XD. Synthesis of mesoporous hexagonal boron nitride fibers with high surface area for efficient removal of organic pollutants. Chem. Eng. J. 2014; 243: 494–499.

109. Yadav S, Asthana A, Singh AK, Chakraborty R, Vidya SS, Singh A, Carabineiro SAC. Methionine-functionalized graphene oxide/sodium alginate bio-polymer nanocomposite hydrogel beads: synthesis, ısotherm and kinetic studies for an adsorptive removal of fluoroquinolone antibiotics. Nanomaterials. 2021; 11(3): 568-593.

110. Yang L, Zhu YJ, He G, Li H, Tao JC. multifunctional photocatalytic filter paper based on ultralong nanowires of the calcium-alendronate complex for high-performance water purification. ACS Appl. Mater. Interfaces. 2022; 14: 9464–9479.

111. Yang X, Chen Z, Zhao W, Liu C, Qian X, Zhang M, et al. Recent advances in photodegradation of antibiotic residues in water. Chem. Eng. J. 2021; 405: 126806.

112. Yu F, Sun S, Han S, Zheng J, Ma J. Adsorption removal of ciprofloxacin by multi-walled carbon nanotubes with different oxygen contents from aqueous solutions. Chem. Eng. J. 2016; 285: 588–595.

113. Zar JH. Biostatistical analysis, Prentice-Hall, Englewood Cliffs. 1984.

114. Zeidman AB, Rodriguez-Narvaez OM, Moon J, Bandala ER. Removal of antibiotics in aqueous phase using silica-based ımmobilized nanomaterials: a review, Environ. Technol. Innov. 2020; 20: 101030.

115. Zhang J, Lin H, Ma J, Sun W, Yang Y, Zhang X. Compost-bulking agents reduce the reservoir of antibiotics and antibiotic resistance genes in manures by modifying bacterial microbiota, Sci. Total Environ. 2019; 649: 396–404.

116. Zhang LH, He YW, Chen M, Gao M, Qiu TL, Wang XM. Pollution characteristics of antibiotic resistant bacteria from atmospheric environment of animal feeding operations. Huan Jing Ke Xue. 2016; 37: 4531–4537.

117. Zhang T, Yang Y, Gao J, Li X, Yu H, Wang N, et al. Synergistic degradation of chloramphenicol by ultrasoundenhanced nanoscale zero-valent iron/persulfate treatment. Sep. Purif. Technol. 2020; 240: 116575.

118. Zhang X, Lian G, Zhang S, Cui D, Wang Q. Boron nitride nanocarpets: controllable synthesis and their adsorption performance to organic pollutants, Cryst. Eng. Comm. 2012; 14: 4670–4676.

119. Zhao H, Liu X, Cao Z, Zhan Y, Shi X, Yang Y, Zhou J, Xu J. Adsorption behavior and mechanism of chloramphenicols, sulfonamides, and nonantibiotic pharmaceuticals on multi-walled carbon nanotubes. J. Hazard. Mater. 2016; 310: 235–245.

120. Zhao J, Yang X, Liang G, Wang Z, Li S, Wang Z, Xie X. Effective removal of two fluoroquinolone antibiotics by PEG-4000 stabilized nanoscale zerovalent iron supported onto zeolite (PZ-NZVI), Sci. Total Environ. 2020; 710: 136289.

121. Zhong Y, Han L, Yin X, Li H, Fang D, Hong G. Three dimensional functionalized carbon/tin(IV) sulfide biofoam for photocatalytical purification of chromium(VI)-containing wastewater. ACS Sustain. Chem. Eng. 2018; 6: 10660–10667.